Bioactive Materials 5 (2020) 210–218

Contents lists available at ScienceDirect

Bioactive Materials

journal homepage: http://www.keaipublishing.com/biomat

Design biodegradable Zn alloys: Second phases and their significant influences on alloy properties

Zhang-Zhi Shi[a,*], Xi-Xian Gao[a], Hai-Jun Zhang[b,c], Xue-Feng Liu[a,**], Hui-Yan Li[a], Chao Zhou[a], Yu-Xia Yin[a], Lu-Ning Wang[a,***]

[a] Beijing Advanced Innovation Center for Materials Genome Engineering, Beijing Laboratory of Metallic Materials and Processing for Modern Transportation, Key Laboratory for Advanced Materials Processing of Ministry of Education, School of Materials Science and Engineering, University of Science and Technology Beijing, Beijing, 100083, China

[b] Department of Interventional and Vascular Surgery, The Tenth People's Hospital of Shanghai, Tongji University, Shanghai, 200072, China

[c] National United Engineering Laboratory for Biomedical Material Modification, Branden Industrial Park, Dezhou City, Shandong, 251100, China

ARTICLE INFO

Keywords:
Biodegradable Zn alloys
Alloy design
Second phase
Microstructure
Comprehensive properties

ABSTRACT

Alloying combined with plastic deformation processing is widely used to improve mechanical properties of pure Zn. As-cast Zn and its alloys are brittle. Beside plastic deformation processing, no effective method has yet been found to eliminate the brittleness and even endow room temperature super-ductility. Second phase, induced by alloying, not only largely determines the ability of plastic deformation, but also influences strength, corrosion rate and cytotoxicity. Controlling second phase is important for designing biodegradable Zn alloys. In this review, knowledge related to second phases in biodegradable Zn alloys has been analyzed and summarized, including characteristics of binary phase diagrams, volume fraction of second phase in function of atomic percentage of an alloying element, and so on. Controversies about second phases in Zn–Li, Zn–Cu and Zn–Fe systems have been settled down, which benefits future studies. The effects of alloying elements and second phases on microstructure, strength, ductility, corrosion rate and cytotoxicity have been neatly summarized. Mg, Mn, Li, Cu and Ag are recommended as the major alloying elements, owing to their prominent beneficial effects on at least one of the above properties. In future, synergistic effects of these elements should be more thoroughly investigated. For other nutritional elements, such as Fe and Ca, refining second phase is a matter of vital concern.

1. Introduction

Biodegradable metals such as Mg, Fe and Zn have drawn more and more attention in recent years. Compared with Mg and Fe, research on Zn is much less intensive. Zn has a hexagonal close-packed (HCP) structure with lattice parameters of $a = 0.2665$ nm and $c = 0.4947$ nm. Experimentally measured Young's modulus (E) of polycrystalline pure Zn lies within 78–121 GPa, the average of which is 97 ± 14 GPa [1]. E_{Zn} is about 46% of E_{Fe} (= 210 GPa [2]), but about 2 times of E_{Mg} (= 39–46 GPa [3]). So its stress shielding effect lies between them. In the as-cast state, Zn is soft and brittle. Through alloying and hot plastic deformation processing, not only the brittleness of Zn can be eliminated, but also its yield strength can be elevated beyond 200 MPa, suitable for making clinical devices such as bone screws and intravascular stents. Alloying usually introduces second phases in Zn, which greatly influence its comprehensive properties. So controlling second phase is a critical aspect for Zn alloy design. However, previous reviews have not dedicated to this aspect yet.

Solid solubility is an important concern for selecting alloying elements to strengthen metals due to their possible effects of solid solution strengthening and precipitation hardening. For biodegradable metals, the basic requirement of alloy elements is that they should not be highly toxic, which excludes elements such as Pb, Hg, As, Tl and so on. Twenty six nontoxic elements [4] can be considered as alloying elements in biodegradable Zn alloys, which are the focus afterwards. According to phase diagrams, among the major elements in the human body, only Mg has a limited solid solubility in Zn, which reaches its maximum value of 0.4 at.% (or 0.1 wt%) at the eutectic temperature of 364 °C, as shown in

Peer review under responsibility of KeAi Communications Co., Ltd.
* Corresponding author.
** Corresponding author.
*** Corresponding author.
E-mail addresses: ryansterne@163.com (Z.-Z. Shi), liuxuefengbj@163.com (X.-F. Liu), luning.wang@ustb.edu.cn (L.-N. Wang).

https://doi.org/10.1016/j.bioactmat.2020.02.010
Received 22 November 2019; Received in revised form 9 February 2020; Accepted 12 February 2020

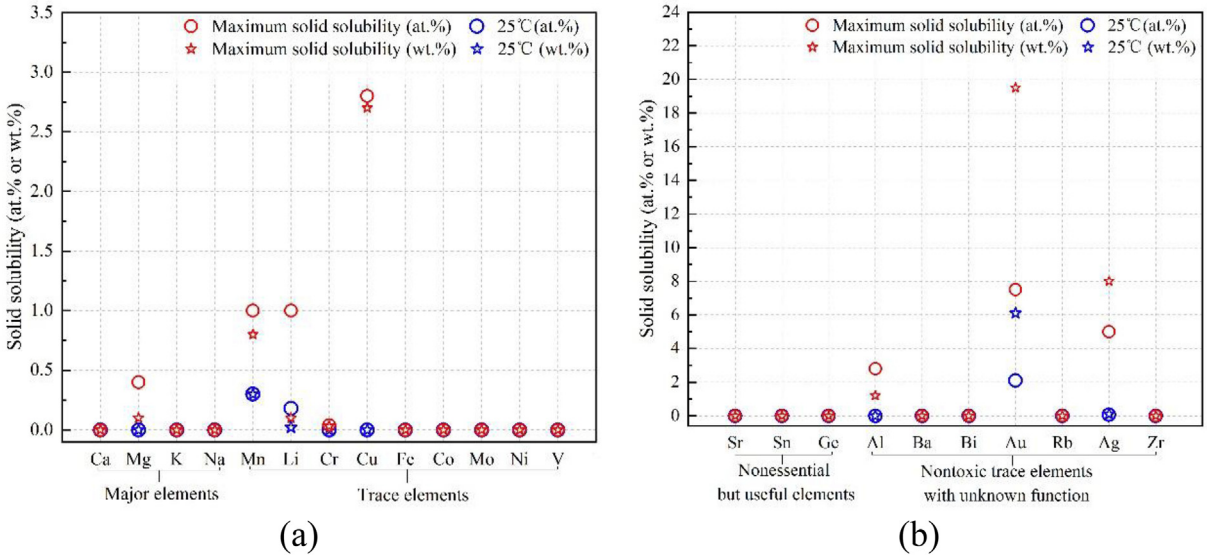

Fig. 1. Solid solubilities of nontoxic alloying elements in Zn: (a) major and trace elements, (b) nonessential but useful elements, and nontoxic trace elements with unknown function.

Fig. 1a. Although the amount of Ca is higher than that of Mg in the human body, Zn alloys with Ca addition are suffered from low ductility, due mainly to the formation of coarse $CaZn_{13}$ particles [5]. Among the trace elements in the human body, only Cu, Mn and Li have solid solubilities in Zn (Fig. 1a). They are ranked decreasingly in the following sequence: Cu (2.8 at.%) > Mn = Li (1.0 at.%) [6–8]. Controversial data of the maximum solid solubility of Li in Zn are published in literatures, which are 1.0 at.% [8] and 3.5 at.% [9]. The former one is more reliable according to the microstructure of Zn-1.1Li alloy (in at.%) that will be discussed later.

None of Sr, Sn and Ge, non-essential but useful elements, has solid solubilities in Zn (Fig. 1b). Among non-toxic trace elements with unknown function, only Au, Ag and Al have solid solubilities in Zn. The solid solubility of Au in Zn is remarkably high, with the maximum value of 7.5 at.% at 483 ˚C and a high value of 2.1 at.% at room temperature. The maximum solid solubility of Ag is 5.0 at.%, while that of Al is 2.8 at.% [10,11]. So addition of Mg, Mn, Li, Cu, Au, Ag or Al is possible to improve mechanical properties of pure Zn through solid solution strengthening and precipitation hardening. Considering cost, Au and Ag are not preferred. Al, also not preferred, has been recognized as a neurotoxicant, possibly relevant to Alzheimer's disease [12,13].

Size and distribution of second phase are also important concerns for alloy design. Uniformly distributed fine second phase particles can significantly reduce pitting damage, and thus improve mechanical integrity during service. The size can be roughly estimated in as-cast state by the reaction during solidification in the Zn-rich end of a phase diagram. Generally speaking, second phase formed due to eutectic reaction is much finer than that formed due to peritectic reaction. The possible alloying elements that can have an eutectic reaction with Zn are summarized in Fig. 2a. Some of them form an eutectic structure of Zn and an intermetallic compound, including Mg, Mn, Li and Cr. The others form an eutectic structure of Zn and a simple substance, including Sn, Ge, Al and Bi. Much more elements have a peritectic reaction with Zn. Those with solid solubilities in Zn are summarized in Fig. 2b, including Cu, Au and Ag. The others without solid solubility in Zn are summarized in Fig. 2c with a stoichiometric γ phase and in Fig. 2d with a non-stoichiometric α phase. When the reaction of L→L + α or L→L + γ takes place, the primary solidification phase (i.e., α or γ phase) is often coarse and dendrite-like intermetallic compound under conditions of conventional casting [14–17]. For the elements without solid solubility in Zn, such as Ca and Fe, the sizes of coarse particles can only be reduced mechanically through plastic processing. In this case, cracks within the particles and weak interfaces between the particles and Zn matrix are prone to promote unstable crack propagation, which is likely to be blamed for decreased ductilities of Zn alloys containing Ca or Fe.

In order to design biodegradable Zn alloys with good comprehensive properties, nutritional or at least non-toxic elements that have solid solubilities in Zn and are related to an eutectic reaction are to be given top priority for being the major alloying elements in pure Zn. These elements are Mg, Mn and Li. For the elements with solid solubilities in Zn that are related to an peritectic reaction, long time and multi-stepped heat-treatments can be employed to change size, distribution and interfaces of second phase particles dramatically through phase transformations. So Cu, Ag and Au are also good choices for alloying.

2. Second phases in biodegradable Zn alloys

2.1. Mg-containing Zn alloys

Mg_2Zn_{11} with a cubic lattice structure (a = 0.8552 nm) is a main second phase in Zn alloys containing Mg [21,22]. Improved corrosion resistance of Zn–5Al–2Mg alloy may attribute to dispersed Mg_2Zn_{11} particles [23]. Minor Mg addition as low as 0.08 wt% (or 0.2 at.%) can strengthen Zn remarkably [24], the mechanism of which is still unclear. Unfortunately, Zn–Mg alloys are suffered to prominent natural brittleness due to precipitation of nano-sized Mg_2Zn_{11} particles and continued static recrystallization in shear bands [25,26]. After a storage of 9 days, elongation of drawn Zn-0.08 Mg wires decreases by about 57% [24], undermining its attractiveness to commercial applications.

2.2. Mn-containing Zn alloys

As shown in Fig. 3a, $MnZn_{13}$ with a base-centered monoclinic (BCM) lattice structure (a = 1.3483 nm, b = 0.76626 nm, c = 0.5134 nm, α = 90˚, β = 127.78˚, γ = 90˚) is a main second phase in Zn alloys containing Mn [27,28]. {110} twinning is an important deformation mode in $MnZn_{13}$. The disorientation angle between the parent and the twin is calculated to be 71.44˚, agreeing well with electron backscattered diffraction (EBSD) measurements [29]. The twinning is beneficial to release accumulated stress in the vicinity of the interface between a hard $MnZn_{13}$ particle (168.2 HV) and its surrounding soft Zn matrix (31.8 HV), which possibly delays cracking. $MnZn_{13}$ particles stimulate recrystallization of Zn grains during plastic deformation not only at high temperatures but also at room temperature, resulting in

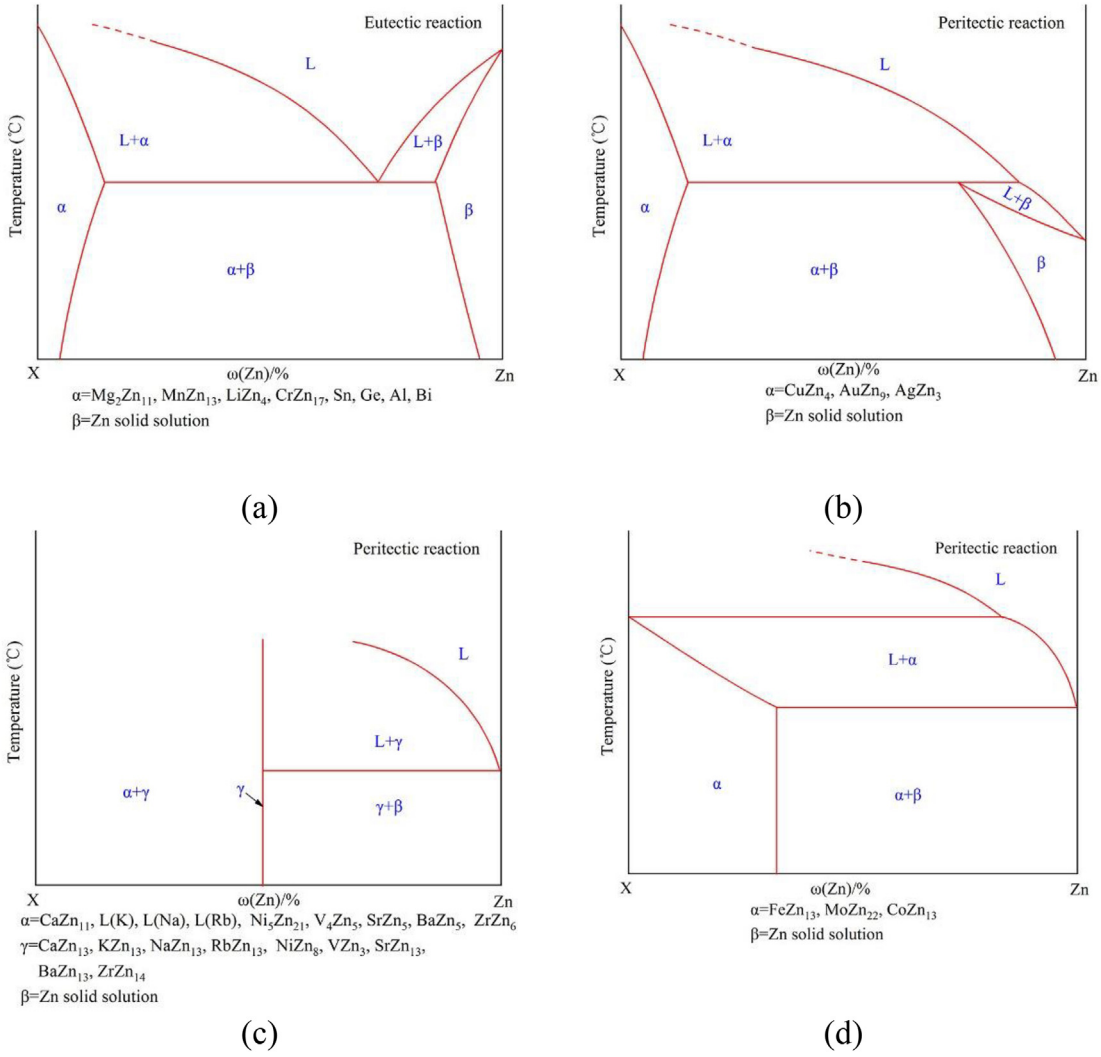

Fig. 2. Summary of Zn-rich ends of binary Zn diagrams: (a) Eutectic phase diagram. (b) Peritectic phase diagram with solid dissoluble element *X*. (c) Peritectic phase diagram with solid indissoluble *X* and a stoichiometric intermetallic compound γ. (d) Peritectic phase diagram with solid indissoluble *X* and a non-stoichiometric intermetallic compound α.

superior ductility of Zn–Mn binary alloys [27]. Precipitation hardening is suggested by the revealing of $MnZn_{13}$ precipitates in heat-treated Zn–Mn binary alloys. The precipitates have a lath-like morphology typically due to solid-state phase transformation, since they exhibit a reproducible orientation relationship (OR) with respect to Zn matrix [30]. Because of very good ductility and potential for precipitation hardening, low-alloy Zn–Mn binary alloys (Mn $<$ 1 wt% or 1.2 at.%) are found to be candidates for developing high-strength low-alloy (HSLA) Zn alloys with good comprehensive properties [28,31].

2.3. Li-containing Zn alloys

β-$LiZn_4$ with a HCP structure (a = 0.278 nm and c = 0.439 nm) is a main second phase in Zn alloys containing Li [18,32,33]. The solid solubility of Zn in β-$LiZn_4$ decreases considerably with decreasing temperature, so that needle-like Zn precipitates form in β-$LiZn_4$ dendrites (Fig. 3b) in as-cast Zn-0.8Li alloy (in wt.%), which endows brittle β-$LiZn_4$ phase a better ductility [18]. Etching solution for microstructure observation is in priority to corrode β-$LiZn_4$ rather than Zn [18]. This is reasonable since the standard electrode potential of Li is much lower than that of Zn. The eutectic composition in the Zn-rich end is 4 at.% (or 0.44 wt%) Li. During solidification of the melt of a hypoeutectic Zn–Li alloy, the primary solidified phase is Zn. When temperature is lowered down to the eutectic temperature of 403 ˚C, Zn/β-$LiZn_4$ eutectic structure (Fig. 3b) forms in the remnant liquid between Zn grains. This kind of microstructure has been reported for Zn-1.1Li and Zn-3.2Li alloys (in at.%) [34]. When the Li content reaches 4 at.%, ideally the microstructure completely consists of Zn/β-$LiZn_4$ eutectic structure. During solidification of the melt of a hypereutectic Zn–Li alloy, the primary solidified phase is β-$LiZn_4$, which would be dendrite-like, as in Zn-5.5Li alloy (in at.%) [34] and in Zn-0.8Li alloy (in wt.% or Zn-7.1Li in at.%) [18].

Another HCP structured phase, α-Li_2Zn_3 (a = 0.4386 nm and c = 1.8738 nm), is detected in as-rolled Zn-0.8Li alloy (in wt.%) by using three-dimensional atom probe (3D-AP) [18]. This metastable phase particles are ellipsoidal shaped with an average long axis of 4.4 nm, resulting in a precipitation hardening effect [18].

2.4. Cu-containing Zn alloys

Controversial results have been reported for the second phase in Zn alloys containing Cu, which is claimed to be ε-$CuZn_4$ [35–37] or ε-$CuZn_5$ [14,38–40]. ε-$CuZn_4$ has a HCP structure (a = 0.27418 nm and c = 0.42939 nm) similar to Zn [35]. However, the crystal structure of ε-$CuZn_5$ has not been provided in references [14,38–40]. According to Zn–Cu binary phase diagram [6], composition of Zn in ε-phase ranges

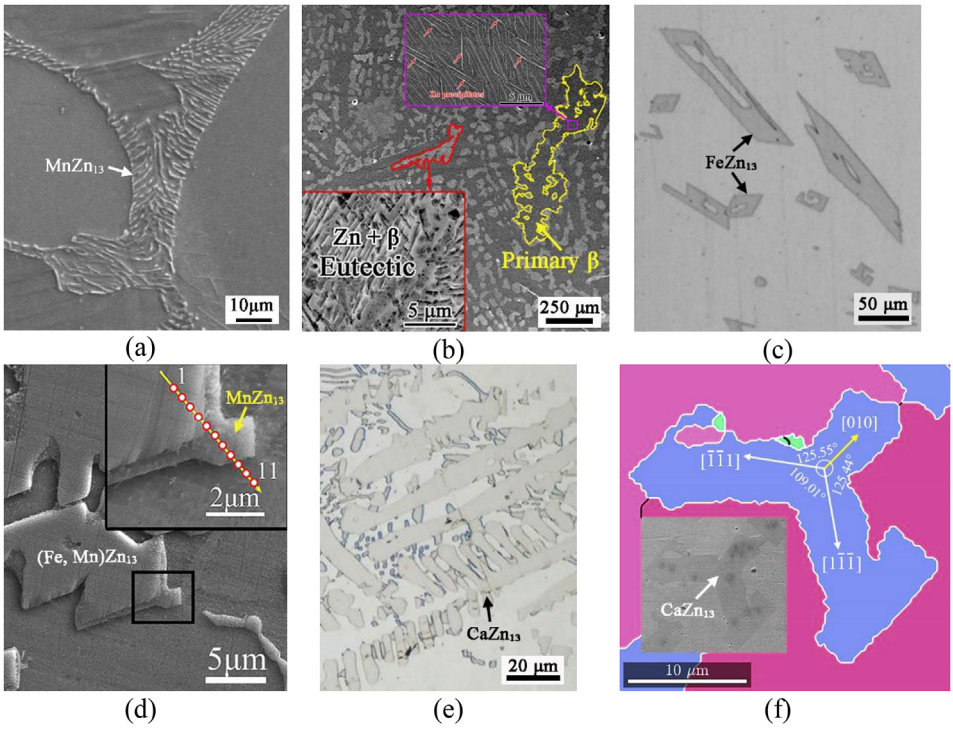

Fig. 3. Second phases in as-cast biodegradable Zn alloys: (a) $MnZn_{13}$ in Zn-0.8Mn alloy; (b) β-$LiZn_4$ in Zn-0.8Li alloy [18]; (c) $FeZn_{13}$ in Zn-0.3Fe alloy; (d) (Fe, Mn)Zn_{13}/$MnZn_{13}$ core/shell particles in Zn–1Mn-0.5Fe alloy [19]; (e) Dendritic $CaZn_{13}$ in Zn-0.8Mn-0.6Ca alloy; (f) Petal-shaped $CaZn_{13}$ in Zn-0.8Mn-0.4Ca alloy [20].

from 78 at.% at 560 ˚C and 88 at.% at 425 ˚C. So Zn/Cu atomic ratio in this phase ranges from 4 to 7. When temperature drops to 200 ˚C, the composition range of Zn in ε-phase shrinks to be 80–86 at.% [6], with Zn/Cu atomic ratio in the range of 4–6. Zn–Cu alloys with Zn as the matrix lie either in the single phase region of Zn solid solution (designated as η in Zn–Cu phase diagram [6]) or in the two-phase region of η + ε. Therefore, at room temperature, the Zn/Cu ratio of ε-phase should be close to 6. This has been confirmed by the measured Zn/Cu ratios of 5.5–6.0 of the second phase particles in as-cast Zn–4Cu alloy (in wt.%) [38]. Increasing the Cu content in the alloy, the material will enter into ε-phase region and then into ε + γ two-phase region, where γ is anther Zn–Cu intermetallic compound. The Zn/Cu ratio of ε-phase in the ε + γ region maintains at 4 from high to low temperatures so that it is more reasonable to describe ε-phase as ε-$CuZn_4$.

The volume fraction of ε-$CuZn_4$ phase increases with increasing Cu addition. In as-cast Zn–1Cu alloy (in wt.%), it is difficult to find this phase by using optical microscopy, although its weak peaks are detected by XRD [38]. However, in as-cast Zn–4Cu alloy (in wt.%), a large amount of $CuZn_4$ dendrites are observed [38]. Small $CuZn_4$ particles effectively refine Zn grains due to good lattice matching between them. As a result, a reproducible OR exists between them, which can be expressed as $[\bar{1}2\bar{1}0]_{CuZn4}//[2\bar{1}\text{-}13]_{Zn}$, $(1\text{–}10\bar{1})_{CuZn4}//(\bar{1}011)_{Zn}$, $(000\text{–}2)_{CuZn4}//(01\text{–}10)_{Zn}$ [35].

2.5. Ag-containing Zn alloys

$AgZn_3$ with a HCP structure (a = 0.28231 nm and c = 0.44407 nm) is a main second phase in Zn alloys containing Ag [10,15]. Owing to good lattice matching, small $AgZn_3$ particles effectively refine Zn grains and exhibit a reproducible OR with respect to Zn matrix, i.e., $[\bar{1}2\text{-}13]_{AgZn3}//[\bar{1}2\text{-}10]_{Zn}$, $(01\text{–}11)_{AgZn3}//(10\text{–}11)_{Zn}$, $(10\text{-}10)_{AgZn3}//(0002)_{Zn}$ [15]. This OR is crystallographically equivalent to that between $CuZn_4$ and Zn, except for the interchange of Zn matrix and the second phase. Since pro-peritectic $AgZn_3$ and $CuZn_4$ particles have similar crystal structures, it is expected that both of them can act as effective heterogeneous nucleation sites for Zn grains. Coarsening of the particles diminishes the grain refining effect. The smallest grain size is obtained at 4.5 wt% Ag or at 2.0 wt% Cu under conventional casting conditions [15,35].

2.6. Fe-containing Zn alloys

As shown in Fig. 3c, $FeZn_{13}$ with a BCM crystal structure (a = 1.3424 nm, b = 0.76080 nm, c = 0.5061 nm, α = 90˚, β = 127.30˚, γ = 90˚) similar to $MnZn_{13}$ is a main second phase in Zn alloys containing Fe [19,41]. However, the coarse Fe-rich phase in Zn-1.3Fe and Zn–4Fe alloys (in wt.%) is claimed to be $FeZn_{11}$ [42,43]. This is doubtful since there is no such phase in Zn–Fe phase diagram [44]. With minor additions of Fe in Zn–1Mn alloy, a new (Fe, Mn)Zn_{13} phase forms [19]. The (Fe, Mn)Zn_{13} particles with a lath-like or a blocky morphology are much larger than $MnZn_{13}$ particles. Since the lattice parameters of (Fe, Mn)Zn_{13} and $MnZn_{13}$ are nearly the same, the latter one can grow epitaxially on the former one, resulting in a (Fe, Mn)Zn_{13}/$MnZn_{13}$ core/shell structure as shown in Fig. 3d [19].

2.7. Ca-containing Zn alloys

$CaZn_{13}$ with a FCC crystal structure (a = 1.213 nm) is a main second phase in Zn alloys containing Ca [20]. It easily grows to be a large dendrite (Fig. 3e). The phase grows preferentially along < 111 > and < 010 > directions, resulting in the formation of 3-petal flower-shaped particles as shown in Fig. 3f. Ca-containing Zn alloys also suffer from the detrimental effect of coarse pro-peritectic $CaZn_{13}$ particles on ductility. In as-cast Zn-0.8Mn-0.4Ca alloy, the average size of $CaZn_{13}$ particles is about 9 times of that of $MnZn_{13}$ particles. Even after large plastic deformation, the former size is still about 5 times of the latter size. In the extruded and then caliber rolled alloy, unbroken large $CaZn_{13}$ particles are severely cracked, which accelerates fracture [20].

3. Combined effects of alloying elements and second phases

An alloying element (designated as X) can significantly change the

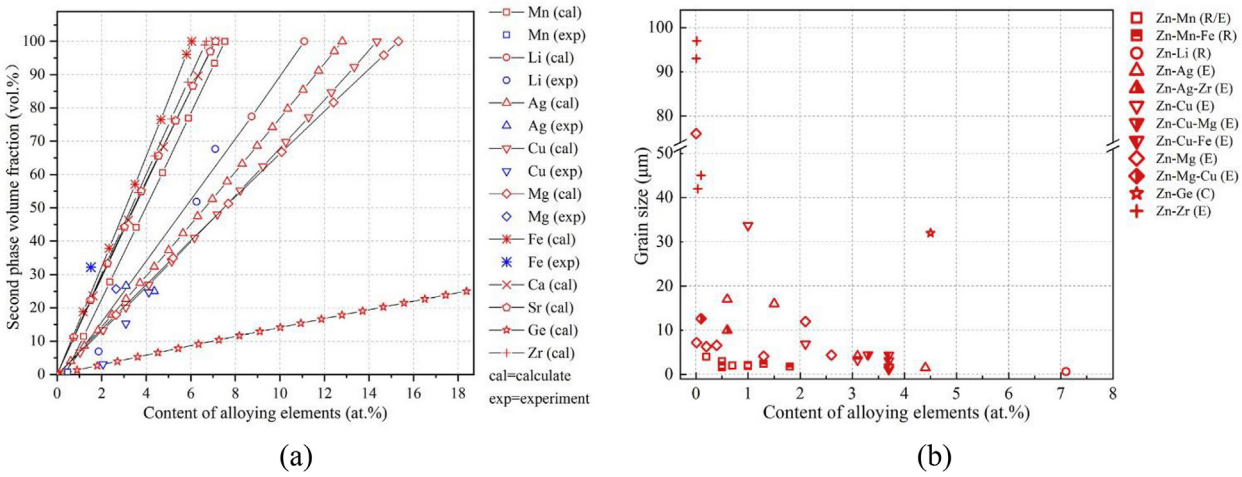

Fig. 4. Biodegradable Zn alloys: (a) Volume fraction (vol%) of second phase at room temperature in function of atomic percentage (at.%). Experimental data are collected from literatures [16,18,27,34,38,42,45,46]. (b) Grain size and content of alloying elements. Data are collected from literatures [16,18,19,24,27,38,41,45,47–52]. C, R and E refer to cast, rolled and extruded, respectively.

microstructure of pure Zn due to formation of Zn-*X* second phase. The equilibrium volume fraction (vol%) of a second phase can be estimated according to its density and Zn-*X* phase diagram [30], as shown in Fig. 4a. When X = Mn, Sr, Ca, Zr or Fe, it forms ZnX_{13} with the highest *X*/Zn atomic ratio. With 6.0–7.5 at.% addition, the volume fraction of ZnX_{13} reaches 100 vol%. When X = Ge, it forms *X* single substance phase with the lowest *X*/Zn atomic ratio of zero. Even with a high addition of 18 at.%, the volume fraction of *X* is still lower than 30 vol%. Experimentally measured volume fractions of second phases have also been presented in Fig. 4a, agreeing well with the calculation. Second phase particles can refine Zn grains [27]. The most effective ones are Mg and Mn. Only 0.5 at.% addition of either of them refines deformed Zn grains to be smaller than 10 μm (Fig. 4b).

3.1. Mechanical properties

Generally for metals, alloying elements increase density of defects hindering dislocation motion, resulting in an improved strength but a decreased ductility. Thus, product of tensile strength and elongation (PSE, in a unit of GPa·%), widely used in researches of steels and Ti alloys [53,54], is employed here to evaluate the comprehensive effect of alloying elements on strength and ductility of Zn, as shown in Fig. 5a. Physically, PSE is close to the area enclosed by a strain-stress curve, i.e., the toughness of a material. It can be seen from Fig. 5a that Mg, Mn, Cu and Li can endow Zn with a PSE > 10 GPa·%. Among them, Mn has the highest efficiency, while Li has the largest effect. With a minor addition of Mn < 1 at.%, PSE of Zn–Mn alloy can reach 17.5 GPa·%, higher than that of 2–4.5 at.% Cu addition. With an addition of 7.1 at.% Li, PSE of Zn–Li alloy jumps to 32.4 GPa·%. Note that fabrication processes influence PSE very much. For a certain Zn alloy, PSE of the as-cast one is often much lower than that of the plastic deformed one, since as-cast Zn alloys are brittle typically with elongations < 3%. According to the physical essence of Young's modulus, alloying will not significantly change E_{Zn} unless second phase particles reach a high volume fraction. For example, *E* of Zn-0.8Cu alloy (in wt.%) is 89 GPa [55], falling in the range of E_{Zn}. Considering most of the second phases in Zn alloys are intermetallics with higher *E* values than E_{Zn}, the most effective strategy to decrease E_{Zn} is to make Zn porous, as done in Ti and Ta for orthopedic implant applications [56,57].

Yield strengths (YS) and Vickers hardnesses of Zn alloys are summarized in Fig. 5b. It can be seen that the latter one is roughly proportional to the former one. However, no certain quantitative relationship has been revealed between them. When X < 6 at.%, the general trend is that YS increases with *X* addition. Among the alloying elements, Mg, Li and Cu have the highest effect of elevating YS. Addition of 3.5–6 at.% Cu or Li rises YS to over 400 MPa with great sacrifice in ductility [34,49]. Mg and Li also have the greatest effect of increasing hardness. Zn-3.94Mg-0.12Mn (in at.% or Zn-1.5Mg-0.1Mn in wt.%) alloy has the highest hardness of about 148.7 HV [69]. According to Fig. 4a, Mg_2Zn_{11} reaches 26.6 vol% in the alloy, which mainly contributes to the high hardness.

3.2. Corrosion rate

Corrosion rates of Zn alloys measured from potentiodynamic polarization test (PPT) and static immersion (SI) are summarized in Fig. 6a, in which over 100 data are collected. The corrosion mediums in the figure include simulated body fluid (SBF), Ringer's solution, Hank's solution, and phosphate-buffered saline (PBS) solution. The alloying element content of pure Zn is zero in the figure. However, it often contains trace impurities [42], which may be blamed for its dispersed corrosion rates. For example, they ranges from below 50 μm/year to over 300 μm/year measured by PPT in Hank's solution (see the hollow squares at 0 wt% in Fig. 6a).

An alloying element with standard electrode potential (E°) lower than that of Zn ($E^\circ_{Zn} = -0.76$ V) is likely to be preferentially corroded, which possibly leads to the formation of a protective passive film on the alloy's surface, resulting in an enhanced corrosion resistance. Li ($E^\circ_{Li} = -3.04$ V), Mg ($E^\circ_{Mg} = -2.37$ V) and Mn ($E^\circ_{Mn} = -1.19$ V) have such an effect (Fig. 6a). Zn-(2–4)Li alloys (in at.% or 0.22–0.44 wt %) exhibit significantly low corrosion rates measured by PPT in SBF, which are about 31–38% of that of pure Zn [34]. The higher the Li content is, the lower is the corrosion rate. Mg has a similar but much weaker effect at high contents (Fig. 6a). Measured by PPT in Hank's solution, extruded Zn-7.7 Mg alloy (in at.% or 3 wt%) exhibits a corrosion rate about 96% of that of extruded pure Zn [50]. When Mg < 7.7 at.%, Zn–Mg alloys corrode faster than pure Zn, due to the noticeable micro-galvanic activity between Mg_2Zn_{11} particles and Zn matrix that exceeds the protection effect of Mg-containing electrochemically inert products formed on the alloy's surface, such as $Mg_2(OH)_2CO_3$ [50]. Analogously, increasing Ca ($E^\circ_{Ca} = -2.87$ V) content, Zn-(0.5–2)Ca alloys (in wt.%) corrode more and more quickly (Fig. 6a), due to increased volume fractions of coarse $CaZn_{13}$ dendrites.

Manufacturing processes, such as rolling, extrusion and drawing, alter the bulk and the surface of Zn alloys, leading to changes in densities of defects (including vacancies, dislocations, and boundaries), orientations of grains and second phases, second phase species, residual stress, and segregation of alloying elements, which will definitely affect

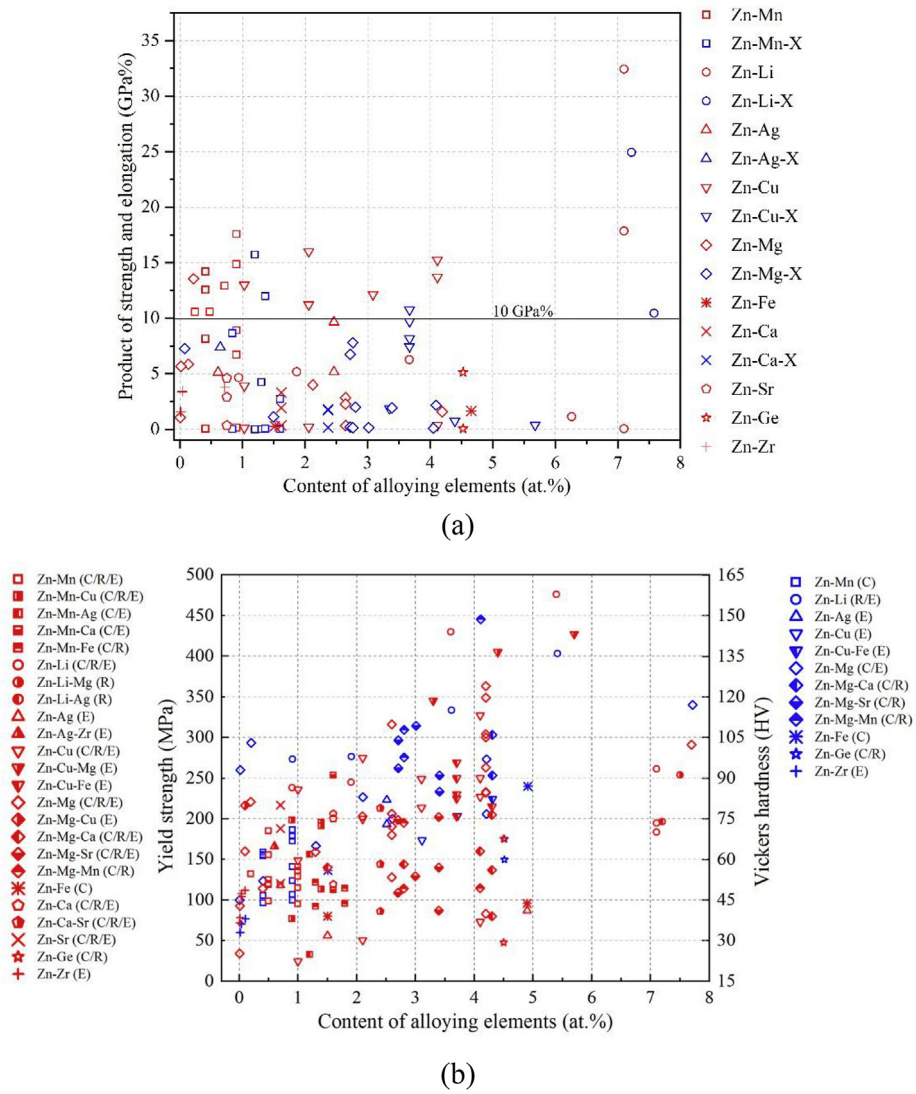

Fig. 5. Biodegradable Zn alloys: (a) Product of tensile strength and elongation (PSE) and content of alloying elements. Binary base alloys are in red, while the others are in blue. Data are collected from literatures [5,18,22,24,27,28,32–34,38,41–43,45,48,49,51,52,58–66]. (b) Yield strength (in red), Vickers hardness (in blue), and content of alloying elements. Data are collected from literatures [5,16,18,19,22,24,27,28,32–34,38,39,41–43,45,46,48–52,58–68]. *X* in (a) and (b) refers to an alloying element. The tensile tests were conducted under uniaxial applied load, at room temperature, with quasi-static strain rates of 3×10^{-4}–8×10^{-3} s^{-1}.

corrosion rate and thereby biocompatibility, however, in a complex way. Although it is in common that hot rolling and extrusion refine Zn grains and second phase particles, contradictory results have been published claiming that these processes can variably increase and decrease corrosion resistance of Zn alloys, which contributes to the data dispersion in Fig. 6a. Extruded Zn-(0.15–3)Mg alloys (in wt.%) [50] and rolled Zn–1Mg-0.1Mn alloy (in wt.%) [66] exhibit lower corrosion rates than their as-cast counterparts, measured by PPT in Hank's solution. This keeps true for the Zn–1Mg-0.1Mn alloy after SI in Hank's solution for 30 days, but not after 90 days [66]. On the contrary, extruded Zn-1.2 Mg alloy [70], rolled Zn–1Mg-0.1Sr and Zn–5Ge alloys (all in wt.%) [52,65] exhibit higher corrosion rates than their as-cast counterparts. A generalized understanding of manufacturing processes on corrosion rates has yet to be presented.

3.3. *In vitro* cytotoxicity

Cell species, alloying elements, extract concentration, and culture time are vital variables for *in vitro* cytotoxicity test of Zn alloys. In order to provide a general overview, an ion concentration factor (ICF) is proposed for statistical analysis on the published data. The ICF is defined by the following equation:

$$\mathrm{ICF} = (w_0 + w_1) \times C \times t, \quad (1)$$

where w_0 is a constant for the influence of Zn matrix, w_1 is contents of alloying elements relevant to micro-galvanic corrosion induced by second phases, C is extract concentration, and t is cell culture time. In general, ICF is proportional to the concentration and action time of released ions. Fig. 6b shows cell viability in function of ICF (in unit of at.%·%·day, and $w_0 = 1$), including 168 data collected from tests of eight kinds of cells. The general trend is that cell viability increases with decreasing ICF. Tolerance of Zn ions is the highest for human osteosarcoma MG63 cells, however, the lowest for murine preosteoblast MC3T3-E1 cells (see hollow squares in Fig. 6b).

Data of the murine fibroblast cell line L929 cells (the red symbols in Fig. 6b) and the human endothelial cell line EA.hy926 cells (the black symbols in Fig. 6b) distribute around inverted C-curves. This kind of shape indicates that the extract concentration exerts the greatest influence on viabilities of the cells. For example, although both the extruded Zn–1Cu alloy (w_1 = 1.03 at.%, C = 100%, t = 1 day) and Zn–3Cu alloy (w_1 = 3.08 at.%, C = 10%, t = 5 days) have almost the same ICFs of 203–204, their EA.hy926 cell viabilities are about 43%

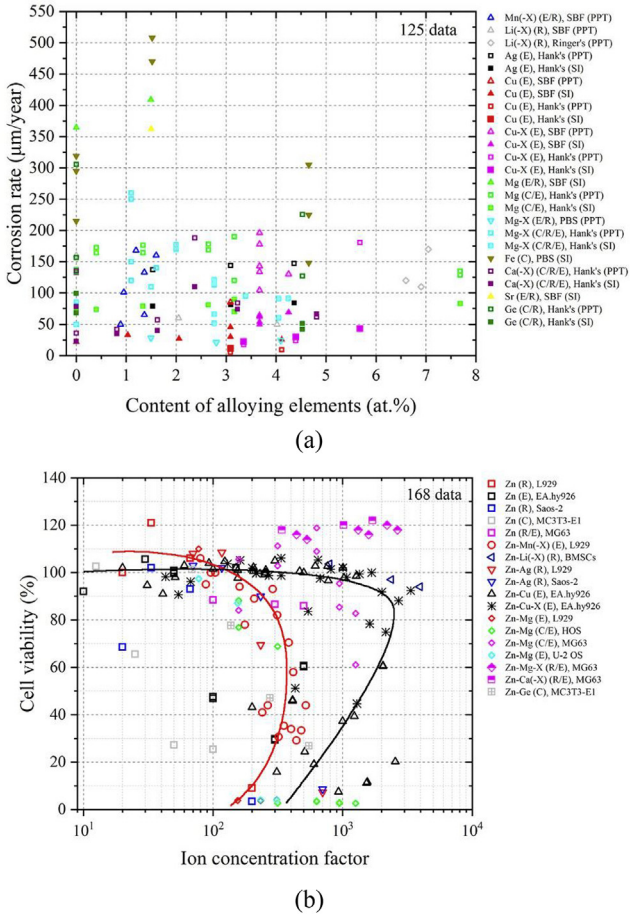

Fig. 6. (a) Corrosion rate and content of alloying elements. SI = static immersion, PPT = potentiodynamic polarization test. Colors differentiate materials, while symbols differentiate corrosion conditions. (b) *In vitro* cell viability and ion concentration factor. Colors differentiate cells, while symbols differentiate materials. Data in (a) and (b) are extracted from literatures [16,19,27,28,32,34,38,39,41–43,49–52,60,61,64–66,70,71]. *X* in (a) and (b) refers to an alloying element. SI and PPT were performed at about 37 °C, in order to simulate the temperature of the human being.

and 101%, respectively [38,49]. The second greatest influence is exerted by contents of alloying elements. For example, pure Zn (w_1 = 0 at.%, C = 33.3%, t = 2 days) with ICF of 66.6 has a high L929 cell viability of about 106%, while Zn–4Ag alloy (w_1 = 2.46 at.%, C = 33.3%, t = 2 days) with ICF of 230 has a much lower L929 cell viability of about 70% [61]. This indicates that Ag has a strong negative effect on proliferation of L929 cells, which is also confirmed by cytotoxicity tests of Zn-0.8Mn-0.4Ag alloy [28]. The third greatest influence is exerted by cell culture time. For example, extruded Zn-3.03Cu-2.64 Mg (in at.% or Zn–3Cu–1Mg in wt.%) alloy has ICF of 332 in two conditions. One is w_1 = 5.67 at.%, C = 10%, t = 5 days, the other is w_1 = 5.67 at.%, C = 50%, t = 1 day. EA.hy926 cell viability in the former condition (i.e., about 99%) is lower than that in the latter condition (i.e., about 106%) [49].

Since MG63 cells have the highest tolerance of Zn ions, it is insensitive to extract concentration. It can be seen from Fig. 6b (the magenta symbols) that additions of Mg, Ca and/or an element *X* (*X* = Sr in the data) promote proliferation of MG63 cells. These alloying elements are well known for their positive effects on proliferation and/or osteogenesis of osteoblast-like cells [72].

4. Conclusions and outlook

Comprehensive properties of biodegradable Zn alloys are determined by their chemical compositions and microstructures. Among 23 nontoxic alloying elements, only 7 elements have solid solubilities in Zn, thus possible for precipitation hardening. The largest solid solubilities (in at.%) of them can be ranked decreasingly as follows: Au > Ag > Cu ≈ Al > Mn ≈ Li > Mg. Since Al is doubted for causing Alzheimer disease, it is not recommended as a preferred alloying element. Au is too expensive to be commercially used. The rest 4 elements (designate as *X*) can form Zn-*X* intermetallic compounds, the efficiency of which, defined by the volume fraction of Zn-*X* per atomic percentage of *X*, is ranked decreasingly as follows: Mn > Li > Ag > Cu > Mg. These elements are considered in priority to be the major alloying elements. Indeed, Mn is the most beneficial for ductility, Mg and Li has the strongest strengthening effects, while Cu achieves a balance of strengthening and toughening effects.

Mg, Mn, Li, Cr and Ge have eutectic reaction with Zn during solidification so that the produced second phase particles are small, which is good for plastic deformation processing, necessary for eliminating brittleness of as-cast Zn alloys. The other nontoxic elements, including nutritional Fe and Ca, are easy to from coarse pro-peritectic Zn-*X* phases, which severely decrease ductility and accelerate corrosion rate. On one hand, the contents of these elements should be carefully controlled. On the other hand, methods should be developed to refine the coarse phases. Recently, minor addition (i.e., 0.06–0.14%) of rare earth elements Y and Nd achieves this goal [73].

The final goal of developing biodegradable Zn alloys is to make clinical devices for curing disease and health recovery. Since the biocompatibility and mechanical properties of pure Zn is more or less clear at the present stage, the effects of alloying elements and second phases should be systematically investigated, the results of which are more valuable when evaluated in larger animals that may more closely approximate the human clinical situation.

Data availability statement

The raw/processed data required to reproduce these findings cannot be shared at this time as the data also forms part of an ongoing study.

Declaration of competing interest

The authors declare that they have no known competing financial interests or personal relationships that could have appeared to influence the work reported in this paper.

Acknowledgement

This work is financially supported by National Key R&D Program of China (2016YFC1102500).

Appendix A. Supplementary data

Supplementary data related to this article can be found at https://doi.org/10.1016/j.bioactmat.2020.02.010.

References

[1] H.M. Ledbetter, Elastic properties of zinc: a compilation and a review, J. Phys. Chem. Ref. Data 6 (1977) 1181–1203.
[2] J.A. Benito, J. Jorba, J.M. Manero, A. Roca, Change of Young's modulus of cold-deformed pure iron in a tensile test, Metall. Mater. Trans. A 36 (2005) 3317–3324.
[3] T. Sumitomo, C.H. Cáceres, M. Veidt, The elastic modulus of cast Mg–Al–Zn alloys, J. Light Met. 2 (2002) 49–56.
[4] Y. Liu, Y. Zheng, X.H. Chen, J.A. Yang, H. Pan, D. Chen, L. Wang, J. Zhang, D. Zhu, S. Wu, K.W.K. Yeung, R.C. Zeng, Y. Han, S. Guan, Fundamental theory of

biodegradable metals—definition, criteria, and design, Adv. Funct. Mater. 29 (2019) 1805402-1-21.
[5] H.F. Li, X.H. Xie, Y.F. Zheng, Y. Cong, F.Y. Zhou, K.J. Qiu, X. Wang, S.H. Chen, L. Huang, L. Tian, Development of biodegradable Zn-1X binary alloys with nutrient alloying elements Mg, Ca and Sr, Sci. Rep. 5 (2015) 10719-1-13.
[6] S.-M. Liang, H.-M. Hsiao, R. Schmid-Fetzer, Thermodynamic assessment of the Al–Cu–Zn system, part I: Cu–Zn binary system, Calphad 51 (2015) 224–232.
[7] H. Okamoto, L.E. Tanner, The Mn-Zn (Manganese-Zinc) system, Bull. Alloy Phase Diagrams 11 (1990) 377–384.
[8] A.D. Pelton, The Li-Zn (Lithium-Zinc) system, J. Phase Equil. 12 (1991) 42–45.
[9] H. Okamoto, Li-Zn (Lithium-Zinc), J. Phase Equilibria Diffus. 33 (2012) 345-345.
[10] T. Gómez-Acebo, Thermodynamic assessment of the Ag-Zn system, Calphad 22 (1998) 203–220.
[11] J.L. Murray, The Al − Zn (Aluminum-Zinc) system, Bull. Alloy Phase Diagrams 4 (1983) 55–73.
[12] R.A. Yokel, The toxicology of aluminum in the brain: a review, Neurotoxicology 21 (2000) 813–828.
[13] R.A. Yokel, The pharmacokinetics and toxicology of aluminum in the brain, Curr. Inorg. Chem. 2 (2012) 54–63.
[14] D. Du, G. Guan, A. Gagnoud, Y. Fautrelle, Z. Ren, X. Lu, H. Wang, Y. Dai, Q. Wang, X. Li, Effect of a high magnetic field on the growth of ε-CuZn5 dendrite during directionally solidified Zn-rich Zn–Cu alloys, Mater. Char. 111 (2016) 31–42.
[15] Z. Liu, D. Qiu, F. Wang, J.A. Taylor, M. Zhang, The grain refining mechanism of cast zinc through silver inoculation, Acta Mater. 79 (2014) 315–326.
[16] M. Sikora-Jasinska, E. Mostaed, A. Mostaed, R. Beanland, D. Mantovani, M. Vedani, Fabrication, mechanical properties and in vitro degradation behavior of newly developed Zn-Ag alloys for degradable implant applications, Mater. Sci. Eng. C 77 (2017) 1170–1181.
[17] Y. Zou, X. Chen, B. Chen, Effects of Ca concentration on degradation behavior of Zn-x Ca alloys in Hank's solution, Mater. Lett. 218 (2018) 193–196.
[18] Z. Li, Z.-Z. Shi, Y. Hao, H.-F. Li, X.-F. Liu, A.A. Volinsky, H.-J. Zhang, L.-N. Wang, High-performance hot-warm rolled Zn-0.8Li alloy with nano-sized metastable precipitates and sub-micron grains for biodegradable stents, J. Mater. Sci. Technol. 35 (2019) 2618–2624.
[19] Z.-Z. Shi, Z.-L. Li, W.-S. Bai, A. Tuoliken, J. Yu, X.-F. Liu, Mn Fe, Zn_{13} phase and its core-shell structure in novel biodegradable Zn-Mn-Fe alloys, Mater. Des. 162 (2019) 235–245.
[20] Z.-Z. Shi, H.-Y. Li, J.-Y. Xu, X.-X. Gao, X.-F. Liu, Microstructure evolution of a high-strength low-alloy Zn–Mn–Ca alloy through casting, hot extrusion and warm caliber rolling, Mater. Sci. Eng. A 771 (2020) 138626-1-11.
[21] P. Villars, Pearson's handbook desk edition, Crystallographic Data for Intermetallic Phases, ASM international, 1997.
[22] L. Yang, P. Guo, Z. Niu, F. Li, Z. Song, C. Xu, H. Liu, W. Sun, T. Ren, Influence of Mg on the mechanical properties and degradation performance of as-extruded Zn-Mg-Ca alloys: in vitro and in vivo behavior, J. Mech. Behav. Biomed. Mater. 95 (2019) 220–231.
[23] C. Yao, S.L. Tay, T. Zhu, H. Shang, W. Gao, Effects of Mg content on microstructure and electrochemical properties of Zn–Al–Mg alloys, J. Alloys Compd. 645 (2015) 131–136.
[24] H.L. Jin, S. Zhao, R. Guillory, P.K. Bowen, Z.Y. Yin, A. Griebel, J. Schaffer, E.J. Earley, J. Goldman, J.W. Drelich, Novel high-strength, low-alloys Zn-Mg (< 0.1wt% Mg) and their arterial biodegradation, Mater. Sci. Eng. C 84 (2018) 67–79.
[25] M.S. Ardakani, E. Mostaed, M. Sikora-Jasinska, S.L. Kampe, J.W. Drelich, The effects of alloying with Cu and Mn and thermal treatments on the mechanical instability of Zn-0.05Mg alloy, Mater. Sci. Eng. A 770 (2020) 138529-1-12.
[26] K. Pieła, L. Błaż, W. Bochniak, P. Ostachowski, M. Łagoda, P. Żabiński, M. Jaskowski, M. Kiper, A. Polkowska, Self-hardening of low-alloyed zinc for biodegradable application, J. Alloys Compd. 810 (2019) 151883-1-9.
[27] Z.-Z. Shi, J. Yu, X.-F. Liu, Microalloyed Zn-Mn alloys: from extremely brittle to extraordinarily ductile at room temperature, Mater. Des. 144 (2018) 343–352.
[28] Z.-Z. Shi, J. Yu, X.-F. Liu, H.-J. Zhang, D.-W. Zhang, Y.-X. Yin, L.-N. Wang, Effects of Ag, Cu or Ca addition on microstructure and comprehensive properties of biodegradable Zn-0.8Mn alloy, Mater. Sci. Eng. C 99 (2019) 969–978.
[29] Z.-Z. Shi, J. Yu, X.-F. Liu, Twinning in $MnZn_{13}$ intermetallic compound with base-centered monoclinic structure in Zn-0.75Mn alloy, Mater. Char. 137 (2018) 9–13.
[30] Z.-Z. Shi, J. Yu, Z.-K. Ji, X.-F. Liu, X.-F. Gu, G. Han, Influence of solution heat treatment on microstructure and hardness of as-cast biodegradable Zn–Mn alloys, J. Mater. Sci. 54 (2018) 1728–1740.
[31] H.-T. Chen, Z.-Z. Shi, X.-F. Liu, Microstructure and mechanical properties of extruded and caliber rolled biodegradable Zn-0.8Mn-0.4Ag alloy with high ductility, Mater. Sci. Eng. A 770 (2020) 138543-1-11.
[32] Y. Zhang, Y. Yan, X. Xu, Y. Lu, L. Chen, D. Li, Y. Dai, Y. Kang, K. Yu, Investigation on the microstructure, mechanical properties, in vitro degradation behavior and biocompatibility of newly developed Zn-0.8%Li-(Mg, Ag) alloys for guided bone regeneration, Mater. Sci. Eng. C 99 (2019) 1021–1034.
[33] S. Zhao, J.-M. Seitz, R. Eifler, H.J. Maier, R.J. Guillory, E.J. Earley, A. Drelich, J. Goldman, J.W. Drelich, Zn-Li alloy after extrusion and drawing: structural, mechanical characterization, and biodegradation in abdominal aorta of rat, Mater. Sci. Eng. C 76 (2017) 301–312.
[34] S. Zhao, C.T. Mcnamara, P.K. Bowen, N. Verhun, J.P. Braykovich, J. Goldman, J.W. Drelich, Structural characteristics and in vitro biodegradation of a novel Zn-Li alloy prepared by induction melting and hot rolling, Metall. Mater. Trans. A 48 (2017) 1204–1215.
[35] Z. Liu, D. Qiu, F. Wang, J.A. Taylor, M. Zhang, Crystallography of grain refinement in cast zinc–copper alloys, J. Appl. Crystallogr. 48 (2015) 890–900.
[36] S.-J. Kim, K.-S. Kim, S.-S. Kim, C.-Y. Kang, K. Suganuma, Characteristics of Zn-Al-Cu alloys for high temperature solder application, Mater. Trans. 49 (2008) 1531–1536.
[37] M. Durman, S. Murphy, An electron metallographic study of pressure die-cast commercial zinc–aluminium-based alloy ZA27, J. Mater. Sci. 32 (1997) 1603–1611.
[38] Z. Tang, J. Niu, H. Huang, H. Zhang, J. Pei, J. Ou, G. Yuan, Potential biodegradable Zn-Cu binary alloys developed for cardiovascular implant applications, J. Mech. Behav. Biomed. Mater. 72 (2017) 182–191.
[39] J.L. Niu, Z.B. Tang, H. Huang, J. Pei, H. Zhang, G.Y. Yuan, W.J. Ding, Research on a Zn-Cu alloy as a biodegradable material for potential vascular stents application, Mater. Sci. Eng. C 69 (2016) 407–413.
[40] Y. Xiao, M. Li, L. Wang, S. Huang, X. Du, Z. Liu, Interfacial reaction behavior and mechanical properties of ultrasonically brazed Cu/Zn–Al/Cu joints, Mater. Des. 73 (2015) 42–49.
[41] R. Yue, J. Zhang, G. Ke, G. Jia, H. Huang, J. Pei, B. Kang, H. Zeng, G. Yuan, Effects of extrusion temperature on microstructure, mechanical properties and in vitro degradation behavior of biodegradable Zn-3Cu-0.5Fe alloy, Mater. Sci. Eng. C 105 (2019) 110106-1-9.
[42] A. Kafri, S. Ovadia, J. Goldman, J. Drelich, E. Aghion, The suitability of Zn–1.3%Fe alloy as a biodegradable implant material, Metals 8 (2018), https://doi.org/10.3390/met8030153.
[43] A. Kafri, S. Ovadia, G. Yosafovich-Doitch, E. Aghion, The effects of 4%Fe on the performance of pure zinc as biodegradable implant material, Ann. Biomed. Eng. 47 (2019) 1400–1408.
[44] K. Han, I. Ohnuma, K. Okuda, R. Kainuma, Experimental determination of phase diagram in the Zn-Fe binary system, J. Alloys Compd. 737 (2018) 490–504.
[45] M. Wątroba, W. Bednarczyk, J. Kawałko, P. Bała, Effect of zirconium microaddition on the microstructure and mechanical properties of Zn-Zr alloys, Mater. Char. 142 (2018) 187–194.
[46] A. Jarzębska, M. Bieda, J. Kawałko, Ł. Rogal, P. Koprowski, K. Sztwiertnia, W. Pachla, M. Kulczyk, A new approach to plastic deformation of biodegradable zinc alloy with magnesium and its effect on microstructure and mechanical properties, Mater. Lett. 211 (2018) 58–61.
[47] S. Sun, Y. Ren, L. Wang, B. Yang, G. Qin, Room temperature quasi-superplasticity behavior of backward extruded Zn–15Al alloys, Mater. Sci. Eng. A 676 (2016) 336–341.
[48] M. Wątroba, W. Bednarczyk, J. Kawałko, K. Mech, M. Marciszko, G. Boelter, M. Banzhaf, P. Bała, Design of novel Zn-Ag-Zr alloy with enhanced strength as a potential biodegradable implant material, Mater. Des. 183 (2019).
[49] Z.B. Tang, H. Huang, J.L. Niu, L. Zhang, H. Zhang, J. Pei, J.Y. Tan, G.Y. Yuan, Design and characterizations of novel biodegradable Zn-Cu-Mg alloys for potential biodegradable implants, Mater. Des. 117 (2017) 84–94.
[50] E. Mostaed, M. Sikorajasinska, A. Mostaed, S. Loffredo, A.G. Demir, B. Previtali, D. Mantovani, R. Beanland, M. Vedani, Novel Zn-based alloys for biodegradable stent applications: design, development and in vitro degradation, J. Mech. Behav. Biomed. Mater. 60 (2016) 581–602.
[51] J. Kubásek, D. Vojtěch, E. Jablonská, I. Pospíšilová, J. Lipov, T. Ruml, Structure, mechanical characteristics and in vitro degradation, cytotoxicity, genotoxicity and mutagenicity of novel biodegradable Zn-Mg alloys, Mater. Sci. Eng. C 58 (2016) 24–35.
[52] X. Tong, D. Zhang, X. Zhang, Y. Su, Z. Shi, K. Wang, J. Lin, Y. Li, J. Lin, C. Wen, Microstructure, mechanical properties, biocompatibility, and in vitro corrosion and degradation behavior of a new Zn-5Ge alloy for biodegradable implant materials, Acta Biomater. 82 (2018) 197–204.
[53] L. Ren, W. Xiao, C. Ma, R. Zheng, L. Zhou, Development of a high strength and high ductility near β-Ti alloy with twinning induced plasticity effect, Scripta Mater. 156 (2018) 47–50.
[54] T. Wang, J. Hu, R.D.K. Misra, Microstructure evolution and strain behavior of a medium Mn TRIP/TWIP steel for excellent combination of strength and ductility, Mater. Sci. Eng. A 753 (2019) 99–108.
[55] C. Zhou, X.Y. Feng, Z.-Z. Shi, C.X. Song, X.S. Cui, J.W. Zhang, T. Li, E.S. Toft, J.B. Ge, L.-N. Wang, H.-J. Zhang, Research on elastic recoil and restoration of vessel pulsatility of Zn-Cu biodegradable coronary stents, Biomed. Tech. (2019), https://doi.org/10.1515/bmt-2019-0025.
[56] A. Bandyopadhyay, I. Mitra, A. Shivaram, N. Dasgupta, S. Bose, Direct comparison of additively manufactured porous titanium and tantalum implants towards in vivo osseointegration, Addit. Manuf. 28 (2019) 259–266.
[57] Q. Han, C. Wang, H. Chen, X. Zhao, J. Wang, Porous tantalum and titanium in orthopedics: a review, ACS Biomater. Sci. Eng. 5 (2019) 5798–5824.
[58] S. Sun, Y. Ren, L. Wang, B. Yang, H. Li, G. Qin, Abnormal effect of Mn addition on the mechanical properties of as-extruded Zn alloys, Mater. Sci. Eng. A 701 (2017) 129–133.
[59] S. Lin, Q. Wang, X. Yan, X. Ran, L. Wang, J.G. Zhou, T. Hu, G. Wang, Mechanical properties, degradation behaviors and biocompatibility evaluation of a biodegradable Zn-Mg-Cu alloy for cardiovascular implants, Mater. Lett. 234 (2019) 294–297.
[60] Z.-Z. Shi, J. Yu, X.-F. Liu, L.-N. Wang, Fabrication and characterization of novel biodegradable Zn-Mn-Cu alloys, J. Mater. Sci. Technol. 34 (2018) 1008–1015.
[61] P. Li, C. Schille, E. Schweizer, F. Rupp, A. Heiss, C. Legner, U.E. Klotz, J. Geisgerstorfer, L. Scheideler, Mechanical characteristics, in vitro degradation, cytotoxicity, and antibacterial evaluation of Zn-4.0Ag alloy as a biodegradable material, Int. J. Mol. Sci. 19 (2018) 755-1-15.
[62] P. Li, W. Zhang, J. Dai, A.B. Xepapadeas, E. Schweizer, D. Alexander, L. Scheideler, C. Zhou, H. Zhang, G. Wan, J. Geis-Gerstorfer, Investigation of zinc-copper alloys as potential materials for craniomaxillofacial osteosynthesis implants, Mater. Sci. Eng. C 103 (2019) 109826.
[63] C. Xiao, L. Wang, Y. Ren, S. Sun, E. Zhang, C. Yan, Q. Liu, X. Sun, F. Shou, J. Duan, H. Wang, G. Qin, Indirectly extruded biodegradable Zn-0.05wt%Mg alloy with

improved strength and ductility: in vitro and in vivo studies, J. Mater. Sci. Technol. 34 (2018) 1618–1627.
[64] H.-F. Li, H.-T. Yang, Y.-F. Zheng, F.-Y. Zhou, K.-J. Qiu, X. Wang, Design and characterizations of novel biodegradable ternary Zn-based alloys with IIA nutrient alloying elements Mg, Ca and Sr, Mater. Des. 83 (2015) 95–102.
[65] X.W. Liu, J.K. Sun, Y.H. Yang, F.Y. Zhou, Z.J. Pu, L. Li, Y.F. Zheng, Microstructure, mechanical properties, in vitro degradation behavior and hemocompatibility of novel Zn–Mg–Sr alloys as biodegradable metals, Mater. Lett. 162 (2016) 242–245.
[66] X.W. Liu, J.K. Sun, F.Y. Zhou, Y.H. Yang, R.C. Chang, K.J. Qiu, Z.J. Pu, L. Li, Y.F. Zheng, Micro-alloying with Mn in Zn–Mg alloy for future biodegradable metals application, Mater. Des. 94 (2016) 95–104.
[67] R. Yue, H. Huang, G.Z. Ke, H. Zhang, J. Pei, G.H. Xue, G.Y. Yuan, Microstructure, mechanical properties and in vitro degradation behavior of novel Zn-Cu-Fe alloys, Mater. Char. 134 (2017) 114–122.
[68] H. Liu, H. Huang, Y. Zhang, Y. Xu, C. Wang, J. Sun, J. Jiang, A. Ma, F. Xue, J. Bai, Evolution of Mg–Zn second phases during ECAP at different processing temperatures and its impact on mechanical properties of Zn-1.6Mg (wt.%) alloys, J. Alloys Compd. 811 (2019) 151987-1-10.
[69] X.W. Liu, J.K. Sun, F.Y. Zhou, Y.H. Yang, R.C. Chang, K.J. Qiu, Z.J. Pu, L. Li, Y.F. Zheng, Micro-alloying with Mn in Zn–Mg alloy for future biodegradable metals application, Mater. Des. 94 (2016) 95–104.
[70] C. Shen, X. Liu, B. Fan, P. Lan, F. Zhou, X. Li, H. Wang, X. Xiao, L. Li, S. Zhao, Mechanical properties, in vitro degradation behavior, hemocompatibility and cytotoxicity evaluation of Zn–1.2Mg alloy for biodegradable implants, RSC Adv. 6 (2016) 86410–86419.
[71] D. Zhu, I. Cockerill, Y. Su, Z. Zhang, J. Fu, K.W. Lee, J. Ma, C. Okpokwasili, L. Tang, Y. Zheng, Y.X. Qin, Y. Wang, Mechanical strength, biodegradation, and in vitro and in vivo biocompatibility of Zn biomaterials, ACS Appl. Mater. Interfaces 11 (2019) 6809–6819.
[72] P.K. Modi, A. Prabhu, Y.P. Bhandary, P.S. Shenoy, A. Hegde, S.P. Es, R.P. Johnson, S.P. Das, S. Vazirally, P.D. Rekha, Effect of calcium glucoheptonate on proliferation and osteogenesis of osteoblast-like cells in vitro, PloS One 14 (2019) e0222240.
[73] Z.-Z. Shi, W.-S. Bai, X.-F. Liu, H.-J. Zhang, Y.-X. Yin, L.-N. Wang, Significant refinement of coarse (Fe, Mn)Zn_{13} phase in biodegradable Zn–1Mn-0.1Fe alloy with minor addition of rare earth elements, Mater. Char. 158 (2019) 109993-1-9.